Received: 8 September 2018 | Revised: 30 October 2018 | Accepted: 12 November 2018

DOI: 10.1002/pip.3100

RESEARCH ARTICLE

WILEY PROGRESS IN PHOTOVOLTAICS

Difference in space-charge recombination of proton and electron irradiated GaAs solar cells

Carmine Pellegrino[1,2] | Alessio Gagliardi[2] | Claus G. Zimmermann[1]

[1] Airbus Defence and Space GmbH, Solar Array Engineering, Taufkirchen, Germany

[2] Institute for Nanoelectronics, Technical University of Munich, Munich, Germany

Correspondence
Claus G. Zimmermann, Airbus Defence and Space GmbH, Taufkirchen 82024, Germany.
Email: claus.zimmermann@gmail.com

Abstract

GaAs component cells, representative of the middle cell in $Ga_{0.5}In_{0.5}P$/GaAs/Ge triple junction solar cells, were irradiated with protons and electrons of various energies and fluences. The local ideality factor, calculated from the measured dark J-V curves, exhibits a characteristic signature of the irradiating particle. With the help of an analytical model based on Shockley-Read-Hall statistics, the recombination current in the space-charge region is calculated, and the local diode ideality factor is reproduced accurately. The inclusion of defect levels away from the intrinsic Fermi level in the bandgap is found to be essential, since a classical two-diode model fails to describe the experimental data. On the basis of literature data of known defect levels in irradiated GaAs, the associated lifetimes and defect introduction rates are derived.

KEYWORDS

GaAs solar cell, ideality factor, radiation induced defects, recombination current, Shockley-Read-Hall recombination, space radiation

1 | INTRODUCTION

Solar cells in the space environment experience electrical performance degradation over time due to the interaction with electrons and protons, trapped in the earth magnetic field, and protons originating from solar flares. In crystalline solar cells, the main cause of degradation due to particle interactions is ascribed to displacement damage, namely the formation of stable defects in the semiconductor crystal lattice as a result of the elastic collision between the impinging particle and the atoms of the target material. For triple junction $Ga_{0.5}In_{0.5}P$/GaAs/Ge solar cells, the current state of the art for space application, it has been well established that the GaAs middle cell is the most radiation sensitive one[1,2] and therefore limits the performance of the whole cell when exposed to space radiation.

In order to make reliable end-of-life (EOL) performance prediction of a solar cell for a given space mission, the continuous electron and proton radiation environment in space has to be condensed into a single quantity, which describes the impact of the radiation spectrum on the solar cell main electrical parameters: the maximum output power P_{mp}, the short-circuit current density J_{sc}, and the open-circuit voltage V_{oc}. A widely used method to achieve this has been developed at the Naval Research Laboratory[3] (NRL) and is referred to as Displacement Damage Dose (DDD) method or NRL method. It makes use of the particle's Non-Ionizing Energy Loss (NIEL). The NIEL represents the amount of energy, which the particle loses upon its trajectory through the target material by creating displacements in the crystal lattice and can be calculated analytically. The total energy deposited in the crystal in form of displacements, the displacement damage dose, is calculated by integrating the NIEL with the particle fluence over all incident energies.

It has been shown in the past, and it is also confirmed for the GaAs cells in this work, that the short circuit current J_{sc} depends primarily on the DDD, irrespective of the fact whether it is introduced by protons or electrons. The impact of radiation on other cell parameters such as the recombination current and the open-circuit voltage V_{oc}, however, depends on the particle type. In these cases, the DDD induced by electrons has to be divided by an equivalence factor R larger than 1 to account for their lower effectiveness compared with protons. This general behavior is expected: the carrier lifetime and thus the diffusion length in the neutral regions depend primarily on the number of defects and their capture cross sections, resulting in a similar behavior whether the DDD is introduced by electrons or protons. The recombination current in the depleted region and thus V_{oc}, on the other hand, depends sensitively on the energy levels of the defects in the bandgap, which might differ regarding the particle type.

For this reason, in order to facilitate a more detailed understanding of the different effectiveness of a given DDD introduced through protons or electrons, we use a discrete Shockley-Read-Hall (SRH) recombination model in order to simulate the dark current-voltage characteristics (J-V) of irradiated GaAs component cells representative of $Ga_{0.5}In_{0.5}P$/GaAs/Ge solar cells. It will be shown that there is a characteristic signature of the type of radiation in the voltage dependence of the junction ideality factor. By fitting this characteristic curve, it is possible to obtain the introduction rates of different defect levels.

2 | EXPERIMENTAL DETAILS

The samples used in this study were 2 × 2 cm^2 GaAs n^+/p isotype cells, representative of the middle cell in triple junction $Ga_{0.5}In_{0.5}P$/GaAs/Ge solar cell. In isotype cells, the remaining subcells are still present in the device structure, but no p-n junction is formed. Thus, the optical filter effect of the top cell is present, but GaAs is the only electrically active p-n junction. The GaAs middle cell had a nominal thickness of 1.5 μm, with a base doping $N_a \approx 5{\cdot}10^{16}$ cm^{-3}. The $Ga_{0.5}In_{0.5}P$ top cell was 0.6 μm thick. The mobility values for GaAs of μ_n = 8500 cm^2 V^{-1} s^{-1} and μ_p = 400 cm^2 V^{-1} s^{-1} were used for electrons and holes, respectively. Additional information on the device structure can be found elsewhere.[4]

The solar cells were homogeneously irradiated at TU Delft and CSNSM Orsay irradiation facilities with different fluences of protons and electrons at two different energies per particle, as shown in Table 1. The solar cells were then annealed for 48 hours under AM0 condition at a fixed temperature of 25°C and then for 24 hours in dark condition at 60°C, according to the relevant space standard.[5] Before and after the irradiation, the solar cells were characterized at room temperature in terms of dark and light J-V, suns-V_{oc}, external quantum efficiency (EQE), and capacitance-voltage (C-V) characteristics.

The light characteristics were measured using a Keithley 2420 sourcemeter and an AEG triple source solar simulator, calibrated with Casolba 2005 standards. The same sourcemeter was used for the dark J-V measurements. The suns-V_{oc} characteristics were determined using an 808 nm-pulsed diode laser as light source. A Spequest Quantum Efficiency set-up from RERA Solutions was used to measure the EQEs. The C-V measurements were performed using a Hewlett Packard 4192A LF impedance analyzer. The doping concentration and the built-in voltage were extracted by Mott–Schottky plots, to account for possible variations in the junction electric field after irradiation because of potential carrier removal effects.

TABLE 1 Particles, energies, and fluences used in irradiating the GaAs isotype cells

Electron 1 MeV	Electron 3 MeV	Proton 1 MeV	Proton 2 MeV
Φ (cm^{-2})	Φ (cm^{-2})	Φ (cm^{-2})	Φ (cm^{-2})
1E+15	1E+14	5E+10	1E+11
5E+15	1E+15	1E+12	1E+12
1E+16	2E+15	3E+12	2E+12
2E+16	5E+15	1E+13	5E+12
-	1E+16	-	-

3 | DISPLACEMENT DAMAGE DOSE ANALYSIS

A homogeneous distribution of nonionizing damage in the GaAs cell after irradiation is required for the DDD method to be applied correctly. The software SRIM[6] was used to simulate displacements caused by protons impinging on the cell structure and to calculate their penetration depth. The simulation confirmed that protons of all chosen energies fully penetrate the active regions of the cell, creating uniform damage in the GaAs active layer. The same holds true for the electron energies used.

The DDD analysis is carried out for the solar cell short-circuit current density J_{sc} and the open-circuit voltage V_{oc}, according to the measured light J-V characteristics. For each set of irradiation data shown in Table 1, the displacement damage dose is calculated as DDD = NIEL·Φ, where Φ is the fluence and the corresponding NIEL is calculated as follows:

$$NIEL = \frac{N}{A}\int_{E_d}^{E_0} L(E)E\left(\frac{d\rho}{dE}\right)_{E_0} dE. \quad (1)$$

In Equation 1, N is the Avogadro constant, A the atomic mass of the irradiated medium, $d\rho/dE$ is the differential scattering cross section for atomic displacement, depending on the particle type and incoming energy E_0, E_d is the threshold energy for displacement and $L(E)$ is the Lindhard partition function, which quantifies the fraction of the recoil energy E that is transferred into atomic displacements rather than ionizing damage. Further information regarding the NIEL calculation steps can be found in Ref. 7.

The cell degradation data are fitted with the equation

$$\frac{Y}{Y_0} = 1 - C_{e,p}\log\left(1 + \frac{DDD}{D_{crit\_e,p}}\right), \quad (2)$$

where Y is the value of the parameter (either J_{sc} or V_{oc}), Y_0 is the corresponding begin-of-life (BOL) value, and $C_{e,p}$ and $D_{crit\_e,p}$ are the fitting parameters, which describe the shape of the curves for electron and proton degradation. While the threshold energy E_d has a negligible impact on the proton NIEL in the experimentally relevant energy range of 1-10 MeV, it highly affects the electron NIEL in the energy range of 0.5-5 MeV. The electron cell data shown in Figure 1 were fitted best with a threshold energy E_d of 21 eV. The value of E_d = 21 eV has already been used in the literature[8,9] in modelling the degradation of the solar cell output parameters in GaAs component cells and in triple-junction solar cells as well and matches the energy required for formation of antisite defects in GaAs.

The same threshold energy was also used for the separate fit of the proton data according to Equation 2. In both, the electron and the proton fit, the same slope of the curve, $C_p = C_e$ was enforced as boundary condition. In order for the electron and proton curves to collapse, an equivalence factor R, defined as

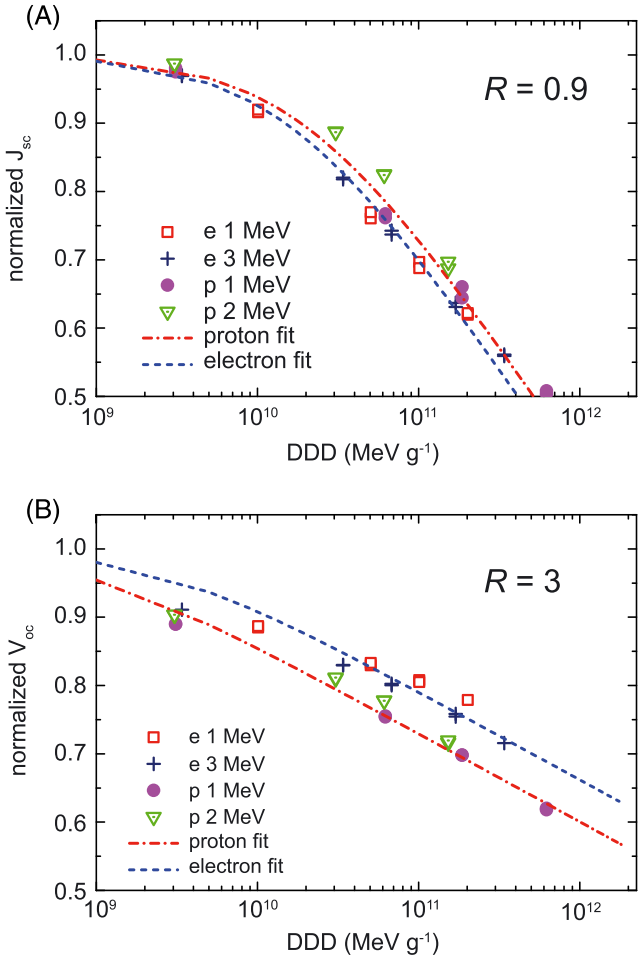

FIGURE 1 Degradation of A, the short-circuit current density J_{sc} and B, the open-circuit voltage V_{oc} as function of the displacement damage dose for GaAs isotype cells, fitted with a threshold energy of E_d = 21 eV. An equivalence factor R of 0.9 and 3 for J_{sc} and V_{oc}, respectively, results in a match of the electron with the proton data [Colour figure can be viewed at wileyonlinelibrary.com]

$$R = \frac{D_{\mathrm{crit_e}}}{D_{\mathrm{crit_p}}}, \tag{3}$$

is introduced in the NRL method. By dividing the electron DDD through R, it is transferred into an equivalent proton DDD, and all data are plotted as a function of the proton DDD. For the GaAs cells irradiated in this work, an R factor of 0.9 is found for J_{sc}, whereas a value of R = 3 results for V_{oc}, as illustrated in Figure 1. For a further investigation into the physical reason behind the different R factors for J_{sc} and V_{oc}, the related microscopic parameters diffusion length $L_{n,p}$ and dark saturation currents J_{01} and J_{02} have to be analyzed in more detail. Neglecting the effect of the cell series and shunt resistances, the dark J-V characteristics are fitted with the two-diode model

$$J = J_{01}\left[\exp\left(\frac{qV}{kT}\right) - 1\right] + J_{02}\left[\exp\left(\frac{qV}{nkT}\right) - 1\right]. \tag{4}$$

n is the junction ideality factor and q, k, and T have their usual meaning. In Equation 4, J_{01} denotes the diffusion component in the quasi-neutral regions of the junction, which can be expressed by the classical Shockley equation[10]

$$J_{01} = \frac{qD_p n_i^2}{L_p N_d} + \frac{qD_n n_i^2}{L_n N_a}, \tag{5}$$

while the term J_{02} accounts for the recombination current originating from the space charge region (SCR).[11]

$D_{n,p}$ denote the diffusivities of electrons and holes and N_d and N_a the doping densities in the n and p region. n_i is the intrinsic carrier density.

A simple model to estimate J_{02} imposes the assumption of a single-level recombination center, located at the midgap position in the SCR. In this case, the junction ideality factor n equals 2, and an expression for the recombination component J_{02} is given in Ref. 12:

$$J_{02} = \frac{\pi\ kTn_i}{2\xi_{av}\tau_{n,p}}. \tag{6}$$

ξ_{av} is the average electric field in the junction, and $\tau_{n,p}$ denotes the mean lifetime of the charge carriers in the SCR.

To unambiguously identify the three dark J-V parameters J_{01}, J_{02}, and n according to Equation 4, the term J_{01} is extracted first through a fit of the suns-V_{oc} curve in the voltage range above 0.7 V. By illuminating the solar cells with a light source and measuring the resulting J_{sc} to V_{oc} pairs, the dark J-V characteristic is obtained as well. Since no current is extracted from the cell during this measurement, however, the series resistance does not play a role. As it will be shown later, in particular the proton J-V curves are dominated by J_{02} up to high currents so it is essential to eliminate series resistance effects in order to access J_{01} at all. The parameters J_{02} and n are then obtained as a result of the dark J-V curve fitting. It is necessary to include the ideality factor n as fitting parameter in Equation 4, which implies that the assumptions made for the modelling of the recombination term in Equation 6 are not valid after irradiation. The diffusion length L_n in the base was determined by fitting the quantum efficiency data of the cells.[11,13]

The DDD analysis is performed on L_n, J_{01}, and J_{02} as illustrated in Figure 2. The degradation curves for L_n^{-2}, J_{01}, and J_{02} follow a linear law, and the fitting is performed with the generalized equation

$$Z = Z_0 + K_Z\ DDD, \tag{7}$$

where Z is the value of the parameter (either L_n^{-2}, J_{01}, or J_{02}), Z_0 is the related BOL value, and K_z is the damage coefficient related to the parameter Z. Again, the GaAs NIEL with a threshold energy E_d of 21 eV was used.

In the case of the diffusion lengths, the proton and electron data collapse in one single curve without the need of any correcting factor, as shown in Figure 2A. This is in agreement with the expected behavior.[14] The identical behavior is observed for J_{01} in Figure 2B. According to Equation 5, however, J_{01} is expected to follow a square root dependence with DDD. It has been already shown in literature, either by device numerical simulation[15] or by experimental data,[16] that the diffusion component of the dark J-V characteristics of irradiated solar cells does not always follow this expected trend. When the diffusion length of the charge carrier in the quasi-neutral region is comparable with the device thickness, a finite surface recombination velocity has to be included in the Shockley diffusion model. Therefore, Equation 5 is no longer strictly valid. Taking in addition a linear increase of the

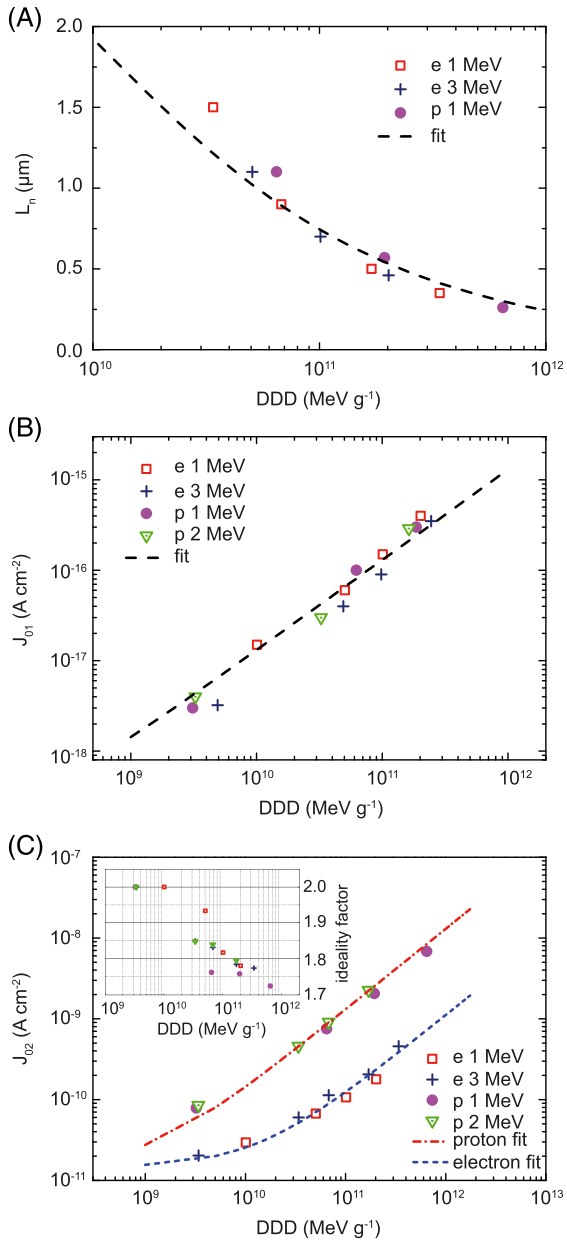

FIGURE 2 Degradation of A, the base diffusion length L_n, B, the diffusion current J_{01}, C, the recombination current J_{02}, and the ideality factor n (inset) as function of the displacement damage dose in GaAs isotype cells, fitted with a threshold energy of E_d = 21 eV [Colour figure can be viewed at wileyonlinelibrary.com]

back-surface recombination velocity with DDD[17] into account, the observed linear dependence can be rationalized.

In the J_{02} case, shown in Figure 2C, however, damage coefficients of 1.3·10^{20} and 1.1·10^{21} A g MeV^{-1} cm^{-2} result for electrons and protons, respectively. In other words, the DDD of electrons is 8.5 times less effective in its impact on J_{02} compared with protons. From this result, a qualitative consideration can be made regarding the degradation of J_{sc} and V_{oc} as well. The current density of the solar cell in short-circuit condition is primarily sensitive to the diffusion length of the minority carriers in the quasi-neutral regions of the p-n junction. Therefore, the independence of L_n on the particle type is consistent with the observed behavior of J_{sc}. On the other hand, the open-circuit voltage has a logarithmic dependence on the generation-recombination current in the depletion region. This current, however, is not only sensitive to the number of displacements but also to the electrical effectiveness of radiation-induced defects as recombination centers in the band gap. As the degradation of J_{02} is different for proton and electron irradiation, an R factor different from 1 is expected for V_{oc} as well.

It is worth noting that the value of n, shown in the inset of Figure 2C, equals 2 for the BOL and low-fluence irradiated cells, whereas it decreases linearly with the displacement damage dose. Hence, the assumption of uniformly distributed defects located at midgap is not valid anymore, and it is necessary to employ a more accurate model in order to describe the recombination current in the dark J-V characteristics.

Since the behavior for protons and electrons appears to be the same regardless of the particle energy, as illustrated for example in Figure 2C, further analysis in this work is carried out for the 1 MeV proton and electron cases. The extracted cell parameters for these particles are summarized in Table 2.

4 | THEORY OF RECOMBINATION IN THE DEPLETION LAYER

The presence of defects in the semiconductor crystal lattice results in allowed energy levels in the bandgap, which act as trapping/detrapping centers. This increases the recombination in the depleted region and affects the dark current of the device. The kinetic of recombination of charge carriers through defect states in the bandgap is exhaustively described by the SRH recombination statistics.[18] Assuming only uniformly distributed recombination centers, in steady-state conditions the recombination rate U for charge carriers is governed by

$$U = \left(pn - n_i^2\right)/[(n + n_1)\tau_p + (p + p_1)\tau_n]. \quad (8)$$

TABLE 2 Diffusion current density J_{01}, recombination current density J_{02}, ideality factor n, and base diffusion length L_n for GaAs isotype cells irradiated with 1 MeV protons and electrons. Data were obtained by fitting the suns-V_{oc}, dark J-V characteristics, and the external quantum efficiency

Irradiation Type	Fluence (cm^{-2})	J_{01} (A cm^{-2})	J_{02} (A cm^{-2})	n	L_n (μm)
BOL	-	1.3E-19	1.9E-11	2	10
e 1 MeV	1E+15	1.5E-17	2.9E-11	2	5
e 1 MeV	5E+15	6.0E-17	6.7E-11	1.93	1.1
e 1 MeV	1E+16	1.5E-16	1.1E-10	1.82	0.7
e 1 MeV	2E+16	4.0E-16	1.8E-10	1.78	0.5
p 1 MeV	5E+10	2.0E-18	7.8E-11	2	8
p 1 MeV	1E+12	1.0E-16	7.5E-10	1.76	1.1
p 1 MeV	3E+12	3.0E-16	2.1E-09	1.75	0.57
p 1 MeV	1E+13	-	6.8E-09	1.72	0.26

The quantities of n, n_1, p, p_1, and E_i can be expressed as:

$$\begin{aligned} n_1 &= n_i \exp\left(\frac{E_t - E_i}{kT}\right); \\ p_1 &= n_i \exp\left(\frac{E_i - E_t}{kT}\right); \\ n &= n_i \exp\left[\frac{q(\psi - \varphi_n)}{kT}\right]; \\ p &= n_i \exp\left[\frac{q(\varphi_p - \psi)}{kT}\right]; \\ E_i &= [E_c + E_v - kTln(N_c/N_v)]/2 = -q\psi. \end{aligned} \tag{9}$$

In Equation 9, n and p are the density of electrons and holes in the conduction and in the valence band, E_i is the intrinsic Fermi level, n_i is the density of electrons and holes in the intrinsic material, φ_p and φ_n are the imrefs (quasi-fermi electrostatic potentials) for holes and electrons, and ψ is the electrostatic potential: $\psi = -E_i/q$. N_c and N_v are the effective densities of state in the conduction and the valence band. n_1 can be interpreted as the density of electrons in the conduction band, if the quasi-fermi level falls at the energy level of the trap E_t. For p_1, the same interpretation holds in terms of holes in the valence band.

TABLE 3 Symbols

Symbol	Quantity
n_1	Density of electrons in the conduction band when the Fermi level falls at E_t
p_1	Density of holes in the valence band when the Fermi level falls at E_t
E_t	Energy level of the recombination centers or traps
n	Density of electrons in the conduction band
p	Density of holes in the valence band
n_i	Carrier density in the intrinsic material
φ_p	Quasi-Fermi electrostatic potential for holes
φ_n	Quasi-Fermi electrostatic potential for electrons
ψ	Electrostatic potential $-E_i/q$
V_{bi}	Built in voltage
E_i	Intrinsic Fermi level
N_c	Effective density of states in the conduction band
N_v	Effective density of states in the valence band
N_t	Density of recombination centers or traps
N_d	Doping density in the n region
N_a	Doping density in the p region
D_n	Diffusivity of electrons
D_p	Diffusivity of holes
τ_{SCR}	Lifetime of electrons and holes injected into the space charge region
c_n	Capture constant for electrons $v_{th,\_n}\sigma_n$
c_p	Capture constant for holes $v_{th,\_p}\sigma_p$
σ_n, σ_p	Capture cross section of a trap for electrons and holes
U_M	Maximum recombination rate value in the space charge region occurring when $\psi = (\varphi_p + \varphi_n)/2$
ξ	Electric field at the junction
W	Space charge layer width
γ	Derivative of the logarithm of the current density with respect to the applied voltage
K	Defect introduction rate
ε	Permittivity

For reference, the definitions of all symbols used in this section are summarized in Table 3.

To simplify the analysis, an equal value of the carrier lifetime for both electrons and holes in the SCR is considered, ie, $\tau_n = \tau_p = \tau_{SCR}$. The electrical effectiveness of a defect state is then characterized by the position of the trap energy level with respect to the intrinsic level $\Delta E_t = E_t - E_i$ and the associated carrier lifetime τ_{SCR}. The latter is expressed by

$$\tau_{SCR} = \frac{1}{N_t c_{n,p}}, \tag{10}$$

where N_t is the defect concentration, and $c_{n,p} = v_{th\_n,p}\cdot\sigma_{n,p}$ is the capture coefficient, determined by the thermal velocity of the carrier $v_{th\_n,p}$ and the capture cross-section $\sigma_{n,p}$. The total current density $J_{r,SCR}$ associated with recombination in the SCR of a p-n junction can be calculated by integrating the recombination rate U over the width W of the SCR

$$J_{r,SCR} = q\int_{W(V)} U(x)dx. \tag{11}$$

U is a function of the position x in the SCR. By combining Equations 8 and 9, the following expression for the recombination rate is derived:

$$U(x) = \frac{\frac{n_i}{\tau_{SCR}}\sinh\left[\frac{q(\varphi_p - \varphi_n)}{2kT}\right]}{\cosh\left[\frac{q}{kT}\left(\psi - \frac{\varphi_p + \varphi_n}{2}\right)\right] + \exp\left[\frac{-q(\varphi_p - \varphi_n)}{2kT}\right]\cosh\left(\frac{E_t - E_i}{kT}\right)}. \tag{12}$$

The spatial dependence of the recombination rate in the SCR is contained in the first hyperbolic cosine term in the denominator of Equation 12. When $\psi = \psi_m = (\varphi_p + \varphi_n)/2$, the recombination rate reaches its maximum value, at a given position x_m in the SCR. Furthermore, Equation 12 quantifies the impact of the defect energy level on the recombination current. The deep states in the gap—with E_t close to E_i—act like efficient recombination centers, thus maximizing the recombination current. Shallower levels with E_t close to E_c or E_v, on the other hand, are less effective.

Integrating Equation 12 according to Equation 11 requires the dependence of the electrostatic potential ψ on the position x in the SCR and the knowledge of ψ_m as well. Assuming at first a symmetrical case, the position $x_m = 0$ corresponds to the metallurgical junction and with $\psi(0) = (\varphi_p + \varphi_n)/2$ in Equation 12 it is possible to evaluate the maximum recombination rate

$$U_M = n_i \exp\left(\frac{qV}{kT}\right) \Big/ \left\{2\tau_{SCR}\left[\exp\left(\frac{qV}{2kT}\right) + \cosh\left(\frac{E_t - E_i}{kT}\right)\right]\right\}. \tag{13}$$

The difference of the two quasi-fermi potentials φ_p and φ_n is given by the externally applied voltage V. For moderate forward bias V smaller than the built in voltage V_{bi}, a linear variation of the electrostatic potential ψ across the SCR can be assumed[12]

$$\psi - \frac{\varphi_p + \varphi_n}{2} = \frac{V_{bi} - (\varphi_p - \varphi_n)}{W}x; \; -\frac{W}{2} < x < \frac{W}{2}. \tag{14}$$

Combining Equations 12 and 14, a more realistic expression is obtained for the recombination rate

$$U(x) = \frac{n_i}{\tau_{SCR}} \frac{\sinh\left(\frac{qV}{2kT}\right)}{\cosh\left[\frac{q(V_{bi}-V)x}{kT\,W}\right] + \exp\left(\frac{-qV}{2kT}\right)\cosh\left(\frac{E_t - E_i}{kT}\right)}. \quad (15)$$

This derivation presented is known as the classical Sah-Noyce-Shockley model.[12]

In order to allow an easier integration of the recombination rate in the SCR, it is common to approximate the function $U(x)$ by combining the maximum recombination rate according to Equation 13 with an exponential decay:

$$U(x) = U_M \exp\left(-\frac{q\xi_{av}}{kT}\frac{1}{\alpha}|x|\right), \quad (16)$$

where α is a constant, which allows the integral over Equation 16 to fit with the one over Equation 15, and ξ_{av} denotes the average electric field in the junction under the assumption of linear potential variation

$$\xi_{av} = \frac{V_{bi}-V}{W} = \sqrt{\frac{q(V_{bi}-V)}{2\varepsilon\left(\frac{1}{N_d}+\frac{1}{N_a}\right)}}, \quad (17)$$

with the permittivity ε. For a symmetrical junction treated in the SNS theory, $\alpha = \pi/2$.[11,12]

The recombination rate in the SCR of an abrupt junction has also been addressed in the literature.[19,20] In an n^+/p junction, the position x_m where the peak of the recombination rate occurs is shifted to the p-type side of the junction. Under the assumption that $N_d >> N_a$, it is possible to calculate the electric field $\xi(x_m)$, at the position where the peak of the recombination rate occurs in the SCR[21,22]

$$\xi(x_m) = \sqrt{2kT\varepsilon^{-1}\left[N_a \ln\left(\frac{N_a}{n_i \exp\left(\frac{qV}{2kT}\right)}\right) - N_a + n_i \exp\left(\frac{qV}{2kT}\right)\right]}. \quad (18)$$

Making again the assumption of a linear potential variation in the SCR, the argument in the brackets of the first hyperbolic cosine term in the denominator of Equation 12 can be written as follows:

$$\psi - \frac{\varphi_p + \varphi_n}{2} = \xi(x_m)\,(x - x_m);\ 0 < x < W, \quad (19)$$

and therefore, Equation 12 becomes for the asymmetrical case

$$U(x) = \frac{\frac{n_i}{\tau_{SCR}}\sinh\left(\frac{qV}{2kT}\right)}{\cosh\left[\frac{q\xi(x_m)}{kT}(x - x_m)\right] + \exp\left(\frac{-qV}{2kT}\right)\cosh\left(\frac{E_t - E_i}{kT}\right)}. \quad (20)$$

Integrating Equation 20 over the SCR allows the evaluation of the total recombination current in the SCR of an asymmetrical p-n junction.[22] Even in this case, however, we resort to an exponential approximation for a more straightforward integration. By making use of the maximum value of the recombination rate in the same fashion as for the symmetrical case, the expression of Equation 20 can be approximated by

$$U(x) = U_M \exp\left(-\frac{q\xi(x_m)}{kT}\frac{1}{\alpha}|x - x_m|\right). \quad (21)$$

For the asymmetrical junction studied in this work, $\alpha = 5\pi/8$ is found, which ensures that the integral of Equation 21 yields the correct value as expressed by the integral of Equation 20. As evident from Figure 3, the exponential approximation of the recombination rate according to Equation 21 fits well the exact value of Equation 20 around $x = x_m$. As the recombination rate is strongly peaked around x_m, the integration according to Equation 11 can be extended from $-\infty$ to $+\infty$, making the total recombination rate independent from the actual value of x_m.

In most p-n junctions, a single-level distribution of defect states located at the intrinsic Fermi level E_i approximates the recombination current in the SCR well. For instance, in a symmetrical case with $E_t = E_i$, integrating Equation 16 over the SCR according to Equation 11 and making use of Equation 13 results in

$$J_{r,SCR} = J_{02}\exp\left(\frac{qV}{2kT}\right) = \alpha\frac{kTn_i}{\xi_{av}\tau_{SCR}}\exp\left(\frac{qV}{2kT}\right). \quad (22)$$

This reproduces the expression stated in Equation 6, which is often used in literature[11] to account for the departure from the Shockley diffusion model ($n = 1$) in diode J-V characteristics. When several traps with different energy levels exist in the forbidden gap, however, Equation 22 does not hold anymore.

The electrical characteristics of the traps have a direct impact on the recombination rate in the SCR. In Figure 4, the maximum recombination rate U_M in the SCR is calculated for a GaAs junction for different values of τ_{SCR} and $\Delta E_t = E_t - E_i$. The dashed curves are obtained keeping a constant value of τ_{SCR} and varying the position of the recombination center in the gap ΔE_t from 0.05 to 0.3 eV. The solid curves are obtained maintaining a fixed value of ΔE_t and decreasing the recombination lifetime from 1 ns to 5 ps. At low voltages, the hyperbolic cosine term in the denominator of Equation 13 dominates, resulting in a slope $n = 1$, whereas at higher voltages the exponential term in the denominator has the larger influence resulting

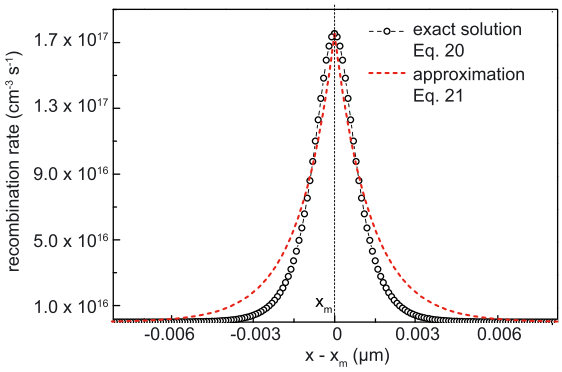

FIGURE 3 Recombination rate as a function of the position $x\text{-}x_m$ in the depletion region for $E_t = E_i$ at an applied bias of 0.3 V. The exact solution of the integral according to Equation 20 is represented by open circles, while the dotted line shows the exponential model proposed according to Equation 21. The electric field at the recombination rate peak $\xi(x_m)$ is calculated using Equation 18 [Colour figure can be viewed at wileyonlinelibrary.com]

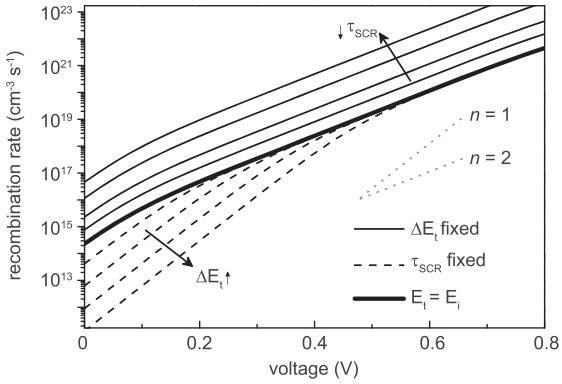

FIGURE 4 Recombination rate as function of the forward bias in a GaAs n^+/p junction, assuming one discrete defect level in the gap. The solid curves are obtained using a fixed τ_{SCR} value and varying ΔE_t. The dashed curves are obtained with a constant value of ΔE_t and by varying τ_{SCR}

in an overall slope of n = 2. In between there is a transition region where Equation 13 is effectively approximated by an exponential law $e^{qV/nkT}$, where n varies between 1 < n < 2. By considering the two asymptotic cases, it is possible to calculate the transition voltage V_{tr} at which the change in slope occurs. As reported Ref. 23 V_{tr} can be estimated by

$$V_{tr} = 2\frac{kT}{q}\left(\frac{|E_t - E_i|}{kT} - \ln 2\right). \tag{23}$$

By varying the position of the defect energy level in the gap, the transition voltage sweeps along the abscissa. The carrier lifetime, on the other hand, has no influence on the slope of the curve. Decreasing the carrier lifetime τ_{SCR} results in an upward shift of the recombination rate.

The recombination current density $J_{r,SCR}$ is then calculated using the expression in Equation 21 and Equation 11. It is important to note that for the given intrinsic carrier concentration of GaAs and the doping levels of the solar cell under test, the voltage dependence of ξ (x_m) in Equation 21 is only contributing to the overall voltage dependence of $J_{r,SCR}$ at bias voltages above 0.8 V. Therefore, the same considerations regarding the slope of U_M are also valid for $J_{r,SCR}$.

With the help of this formalism, it is possible to consider the contributions of discrete energy levels in the band gap of the SCR on the experimentally measured recombination current J_{dark}, provided the diffusion contribution or a series resistance effect are not affecting the overall cell current in the voltage region of interest. Since the energy level of the trap is determining the voltage at which a change in the slope of the recombination current occurs, it is convenient to define a new parameter γ

$$\gamma = \frac{d[\ln J_{dark}(V)]}{dV}, \tag{24}$$

which is highly sensitive to this slope change thanks to using the derivative of the logarithm of the dark saturation current with respect to voltage. The parameter is directly related to the local value of the ideality factor n via

$$n = q\,(kT\gamma)^{-1}. \tag{25}$$

Consequently, for a two-diode model and a single-level defect, γ is constant at a value of $q\cdot(kT)^{-1} \simeq 39$ in the diffusion regime (n = 1) and assumes a value of $q\cdot(nkT)^{-1}$ for the recombination regime. In the latter case, for the standard SRH recombination model with $E_t = E_i$, n = 2, and $\gamma \simeq 19$ results. Therefore, the value of γ is expected to remain constant around 19 in the recombination regime and then to increase to 39 as soon as the diffusion regime dominates at higher forward bias.

When more than one defect contributes concurrently to the overall current density, they are clearly revealed in the local value of γ. As an example, a simulation of the J-V characteristic of a GaAs p-n junction is shown in Figure 5, considering two discrete defect states at $E_{t,1} = E_i$ and $E_{t,1} = E_i + 0.25$ eV. The total current density of the device is calculated as follows:

$$J_{tot} = J_{diff} + J_{r1,SCR} + J_{r2,SCR}, \tag{26}$$

where J_{diff} is the diffusion component expressed by the Shockley equation, while $J_{r1,SCR}$ and $J_{r2,SCR}$ are the recombination current contributions related to the two defects. On the basis of the individual plots of these contributions as shown in Figure 5, two main regimes can be identified. In the low-bias region below 0.7 V, the current due to recombination in the SCR dominates. For higher bias voltages, the diffusion component dominates the recombination current, and the ideality factor approaches one. As the current increases, the effect of the series resistance appears, resulting in a decrease of γ again at high voltages. In the recombination regime, the electrical characteristic of the defects completely determine the γ-V curve. For a single defect level, there is only a change in the slope from n = 1 to n = 2 at a voltage, which is governed solely by the energy level of the defect according to Equation 23. For this example, at ≈0.1 V for the $E_{t,1} = E_i$ defect and ≈0.45 V for the $E_{t,1} = E_i + 0.25$ eV defect. In the combination of two defect levels, however, it is possible to reach a turning point in the γ-V curve as shown in the inset of Figure 5. Its position is again determined by the energy level of the defect with the larger ΔE_t. The τ_{SCR} associated with the traps results in a parallel shift of

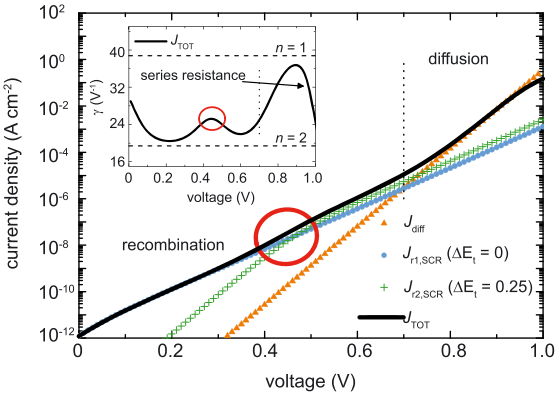

FIGURE 5 Simulated J-V characteristic of a GaAs n^+/p junction. The recombination current in the SCR is due to two defect levels in the gap, with different values of τ_{SCR} and with energy levels $E_{t,1}$ close to E_i (light blue dots), and $E_{t,2}$ shifted 0.25 eV from E_i (green crosses). The contribution of the series resistance and the diffusion component (orange triangles) are included in the model. The slope of the logarithm of the current as function of the applied bias is shown in the inset [Colour figure can be viewed at wileyonlinelibrary.com]

the current density-voltage curves associated with the traps, and this mainly affects the peak height in the γ-V curve.

Even though the density of energy states in the gap is continuous in nature, a discrete analysis already proved to be of interest in Ref 23,24. The model employed in this work yields information inherent to the electrical effectiveness of defects that are present with high-concentration level. The parameter γ is sensitive to changes in the slope of the dark current, which are in turn completely determined by the electrical characteristics of the defects in the SCR. Therefore, the electrical effectiveness of defects can be extracted from the voltage dependence of the parameter γ, under the assumptions that

1. defects can be treated as discrete levels in the forbidden bandgap, homogeneously distributed in the SCR, acting as traps for charge carriers;
2. traps in the gap act as nonradiative recombination center when the junction is forward biased;
3. the contribution of each discrete level to the overall current density can be taken into account separately;
4. the diffusion component or series resistance is not affecting the total current density in the voltage region of interest, and the recombination current in the SCR is the dominating contribution.

The downside of this approach is the intrinsic inability to discern whether a defect state acts as electron trap or hole trap. The effect of the defect energy level in terms of recombination current is symmetrical around the midgap; eg, an electron trap with high-capture coefficient c_n located above the intrinsic level would have the same effect as an hole trap with a high c_p value, located symmetrically below E_i. In the depletion layer of a p-n junction, both electron and hole traps are a source of recombination and contribute together to the overall current density.

5 | EXPERIMENTAL RESULTS AND DISCUSSION

The analytical model of recombination in the SCR is now applied to the measured dark J-V characteristic of the 1 MeV proton and electron irradiated GaAs solar cells. In Figure 6, the γ characteristics measured for the BOL cell (open squares), and the simulation (dashed black curve) is shown. In this case, a good match is achieved using the parameter J_{01}, J_{02}, and n extracted by fitting of the dark J-V and the suns-V_{oc} characteristic with Equation 4. The value of γ stays close to the value consistent with n = 2 in the low-bias regime. At very low voltage, a slight downward bending below the level of n = 2 is found, and it is attributed to the nonuniformity of defect states in the SCR, as reported in Ref. 24.

As the voltage increase, both the recombination current in the SCR and the diffusion component in the neutral regions are significantly contributing to the overall current density and thus $q\cdot(kT)^{-1} < \gamma < q\cdot(2kT)^{-1}$. The diffusion component starts to affect γ at high-bias voltage (>0.8 V) until it takes over the recombination regime. As the total current value increases at higher bias voltage, the effect of the series resistance starts to bend the BOL curve downward, and this effect is not included in this simulation.

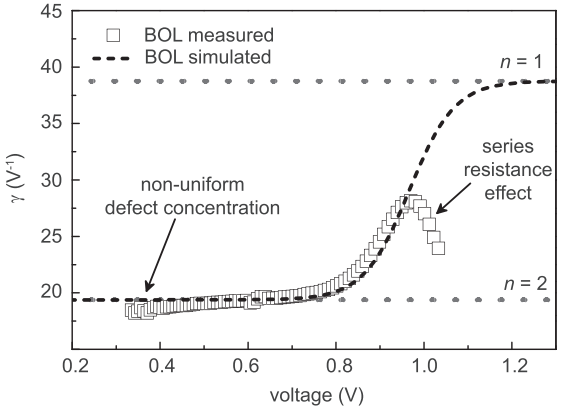

FIGURE 6 Derivative of the logarithm of the current density with respect to the applied voltage (γ curve) for measured (open squares) GaAs isotype cells at BOL. The black dashed curve represents the fit with the two-diode model

The BOL cell represents the case where the two-diode equation appropriately describes the behavior of the current density, with the recombination component evaluated with the single level, midgap assumption. The same analysis is performed for irradiated cells with protons and electrons at 1 MeV energy. The measured γ characteristics are shown for all fluence values in Figure 7. The dashed curves in Figure 7 are numerically calculated for one fluence value from the

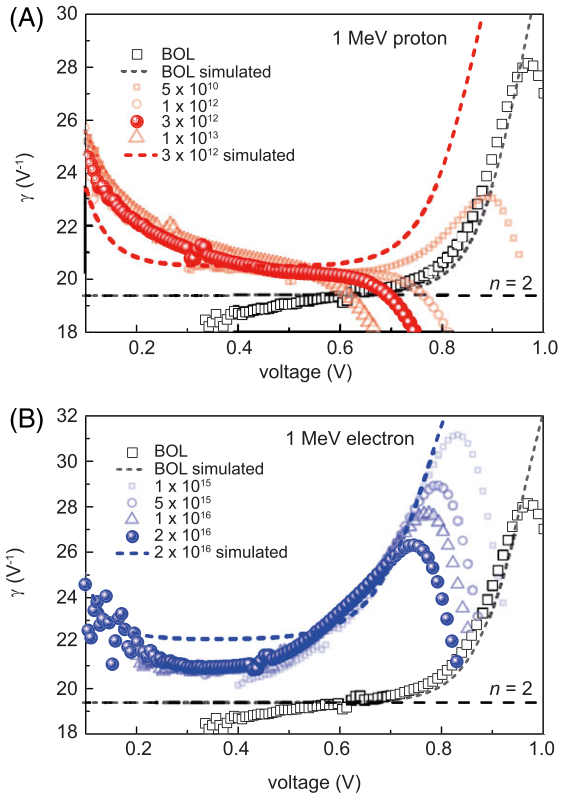

FIGURE 7 Measured A, proton and B, electron γ-V curves. The solid spheres corresponds to a proton fluence of $\Phi = 3\cdot10^{12}$ cm^{-2} and an electron fluence of $\Phi = 2\cdot10^{16}$ cm^{-2}, respectively. These result in a comparable displacement damage dose DDD ≈ $2\cdot10^{11}$ MeV g^{-1}. The BOL curves are also superimposed with black squares for comparison. The dashed curves represent the fit with the two-diode model parameters [Colour figure can be viewed at wileyonlinelibrary.com]

simulated dark J-V using the parameters J_{01}, J_{02}, and n extracted by fitting of the measured characteristics with the two-diode model according to Equation 4.

It is remarkable how proton and electron irradiation leave a particular signature in the γ-V curve of the solar cells. For the proton irradiation in Figure 7A, a steep inverse slope marks the low bias region, while apart from the lowest fluence case, no positive value of dγ/dV is found. For electrons Figure 7B, on the other hand, the departure of the value of γ from the case where $n \simeq 2$ occurs at lower voltage (>0.5 V) than in the BOL case (>0.8 V). The slope of the γ-V characteristic is, however, much lower than in the case of the ideal two-diode model according to Equation 4. Even taking into account that the effect of series resistance in the high bias region is neglected here, the γ-V plot clearly reveals that the two-diode model according to Equation 4 is poorly describing the recombination mechanisms in the SCR of the cells.

Therefore, the overall dark current density including the component due to the recombination in the SCR is modelled as follows:

$$J_{dark} = J_{diff} + J_{r,SCR} = J_{01}\left[\exp\left(\frac{qV}{kT}\right) - 1\right] + \sum_n q\int_{W(V)} U(x)_n dx, \quad (27)$$

where $U(x)_n$ are the recombination rates associated with the n-th state in the gap, according to Equations 13 and 21. To enable an unambiguous fit of the recombination current in the depleted region in the low bias region, J_{01} is extracted from the suns-V_{oc} measurement at high-bias voltages. The corresponding values have already been summarized in Table 2. A common value for the series resistance* of R_s = 1 Ω cm^2 is adopted in the model for all cells, which is in agreement with values reported in literature for the same type of cells.[25] The carrier removal effect after irradiation does not induce any significant effect in terms of the electric field strength for the two cases studied, and is thus neglected. The γ-V curve is the central functional dependence for the fitting process. Because of the differential nature of the γ parameter, an integration is required to arrive at absolute values of the dark current again. This constant is obtained by a final fit of the model to the measured dark J-V curve. This results then in absolute values of τ_{SCR} according to Equation 13.

There are two main parameters in Equation 13 that need to be determined: the carrier lifetime $\tau_{SCR,n}$ as well as the energy level ΔE_t of the defects. The energy levels of the defects introduced by particle irradiation are extracted from published deep-level transient spectroscopy (DLTS) data in the literature. For electron and hole traps in both n- and p-type GaAs following 1 MeV electron irradiation, several references are available.[26-28] For 1 MeV proton irradiation, several authors reported their results for high-energy proton irradiation on n-type GaAs.[24,29] Therefore the fitting procedure according to Equation 27 is solely varying the carrier lifetimes $\tau_{SCR,n}$ associated with the n-th defect level. Table 4 lists the defect levels used as well as the carrier lifetimes adopted as a result of the fitting process.

The fitting process is quite robust. In order to reproduce accurately the shape of the γ-curves, all defect levels shown in Table 4 have to be included in the model. For instance, the stepwise fitting

*extracted from the dark J-V characteristics of irradiated samples, measured under high-current bias condition.

TABLE 4 Defect lifetime τ_{SCR} used in the simulation of the dark J-V and γ-V characteristic of GaAs isotype cell after irradiation with protons and electrons at 1 MeV energy. The defect energy levels are measured with DLTS in Ref. 24,26-29

		Defect Label			
		PR1	PR2	PR2'	PR3
		$\lvert E_t - E_i\rvert$ (eV)			
Irradiation type	Fluence (cm^{-2})	0.03	0.07	0.15	0.22
		τ_{SCR} (ns)			
p 1 MeV	5E+10	6.30	10	25	5
p 1 MeV	1E+12	0.30	0.48	1.20	3
p 1 MeV	3E+12	0.10	0.30	0.40	1
p 1 MeV	1E+13	0.04	0.06	0.08	0.12
		Defect Label			
		H4	H5	H3	H2
		$\lvert E_t - E_i\rvert$ (eV)			
Irradiation type	Fluence (cm^{-2})	0.04	0.10	0.21	0.33
		τ_{SCR} (ns)			
e 1 MeV	1E+15	10	-	-	30
e 1 MeV	5E+15	4.5	18	18	6.7
e 1 MeV	1E+16	2	10	10	3
e 1 MeV	2E+16	1	3	4	1

for the cell irradiated with 1 MeV electron at a fluence of Φ = 10^{16} cm^{-2} is illustrated in Figure 8, including progressively the defects H4, H5, H3, and H2 in Equation 27. Each defect contributes mainly around its voltage region of interest (transition voltage V_{tr}), and the γ-curve is accurately reproduced only when all four levels are included in the model.

In Figure 9, the measured and simulated dark J-V characteristics and the γ-V characteristics are illustrated. Unlike with the simple two-diode model according to Equation 4, a very good fit to the experimental curves is obtained for all proton and electron data.

If the capture cross-section value for a defect σ and the thermal velocity v_{th} are known, it is possible to calculate the actual defect concentration N_t from the associated lifetime $\tau_{SCR,n}$ by inverting the

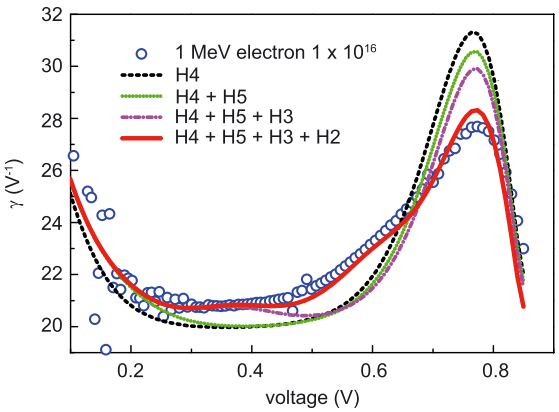

FIGURE 8 Stepwise fitting of the γ-curve for 1 MeV electron irradiated GaAs cell with 10^{16} cm^{-2} fluence, using in sequence the traps H4, H5, H3, and H2. A series resistance R_s = 1 Ω cm^2 and a diffusion component J_{01} = 1.5·10^{-16} A cm^{-2} are adopted in this case [Colour figure can be viewed at wileyonlinelibrary.com]

relation in Equation 10. It is then possible to quantify the introduction rate K for each irradiation-induced defect, defined as follows:

$$K = \frac{dN_t}{d\Phi}. \tag{28}$$

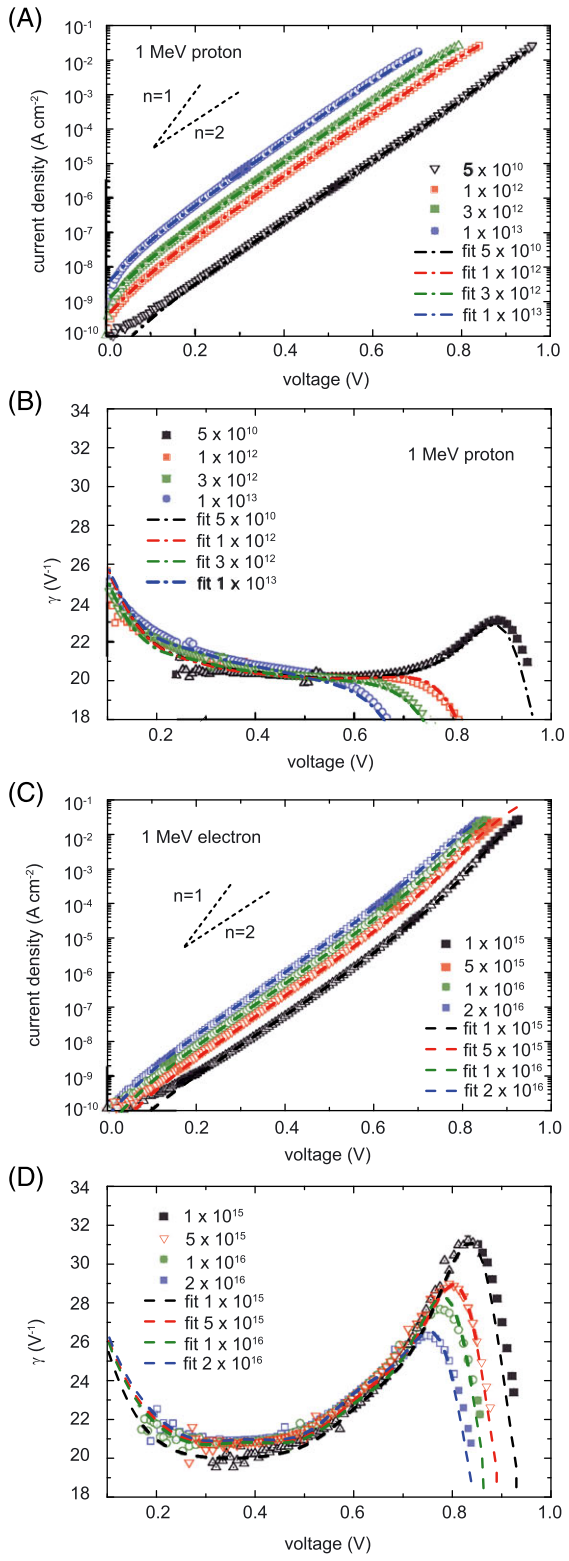

FIGURE 9 Fitting of the dark J-V characteristics and of the derivative of the logarithm of the current density (γ characteristic) for 1 MeV proton A, B, and 1 MeV electron C, D, irradiated GaAs isotype cells [Colour figure can be viewed at wileyonlinelibrary.com]

In p-type GaAs, good literature data exist for the defect introduction rates for the H4 and H5 levels through 1 MeV electron irradiation.[27] For a consistency check, the defect introduction rate has been evaluated based on the electron data according to Table 4. Literature data were used for the capture cross-section σ of the defects induced by 1 MeV electron irradiation.[24,26-28] For the levels H5 and H4, the defect concentrations at various fluences are extracted, and the introduction rates K are calculated as the slope of the linear fits shown in Figure 10. The value obtained, listed in Table 5, are in good agreement with the range already reported in literature for these type of defects.[27]

Finally, in order to discuss the difference in the proton and electron data obtained in Table 4, it is instructive to compare the cells with a proton fluence $\Phi = 3{\cdot}10^{12}$ cm^{-2} to the cell with an electron fluence of $\Phi = 2{\cdot}10^{16}$ cm^{-2}. These two particle/fluence combination deposit the same displacement damage dose DDD $\approx 2{\cdot}10^{11}$ MeV·g^{-1} in the crystal. For the three lowest energy levels, the lifetimes in the proton irradiated samples are one order of magnitude smaller than in the electron case. Assuming a comparable capture cross section for proton and electron-induced defects for these levels close to E_i, protons produce one order of magnitude more defects close to the intrinsic level than electrons, with the associated high effectiveness as recombination centers in the SCR. Since the same amount of nonionizing energy is deposited in both cases, a significant amount of electron defects must therefore be distributed in a wider energy range. The dark J-V analysis presented allowed only to access defect levels up to $\Delta E_t \approx 0.35$ eV and therefore no definitive conclusion can be reached here. The fact, however, that in the electron case the lifetimes of the $\Delta E_t = 0.33$ eV level is the same as for the $\Delta E_t = 0.04$ eV level—unlike in the proton case—can be interpreted as a first indication that the energy deposited by electron collisions results in a wider spectrum of significantly contributing energy levels in the gap.

Likewise the combined lifetime in the neutral regions, calculated as inverse sum of the individual lifetimes of the different defect levels, results in a one order of magnitude difference in the $\Phi = 3{\cdot}10^{12}$ cm^{-2} proton case compared with the $\Phi = 2{\cdot}10^{16}$ cm^{-2} electron case. This is not in line with a similar J_{01} measured for these two cases. Again, this difference can only be reconciled assuming that a defect level is

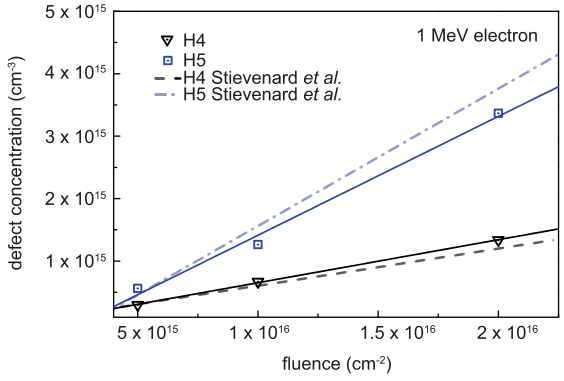

FIGURE 10 Defect concentration for H4 and H5 as function of 1 MeV electron fluence in GaAs isotype cells. The introduction rate is extracted by the slope of the linear fit (solid lines), while the dashed lines represent the related slopes reported in literature[27] [Colour figure can be viewed at wileyonlinelibrary.com]

TABLE 5 Introduction rate K extracted for H4 and H5 after 1 MeV electron irradiation on GaAs isotype cells. The capture cross section and the reference K values are taken from Ref. 27,28

Irradiation Type	Defect Label	$\lvert E_t - E_i \rvert$ (eV)	σ (cm^2)	K Reference (cm^{-1})	K (cm^{-1})
e 1 MeV	H4	0.04	6.8E-14	0.06-0.08	0.07
e 1 MeV	H5	0.10	9E-15	0.22	0.19

introduced by electrons outside the accessible range $\Delta E_t \approx 0.35$ eV with sufficiently short lifetime.

6 | CONCLUSION

The dark J-V curve of irradiated GaAs solar cells cannot be fitted by a classical two-diode model, unless an unphysical exponent n, $1 < n < 2$, is assumed. Even then, the local ideality factor is only reproduced poorly. An analytical approach, involving a discrete multilevel SRH model, however, is able to accurately model the recombination current in the SCR. By making use of known defect levels in GaAs, the introduction rates of the different defects in the SCR can be assessed. In this way, the pronounced difference in the local diode ideality factor between proton and electron irradiated cells is traced back to a different introduction rate of defect levels close to the intrinsic Fermi level. This provides some additional insight into the origin of the proton-electron equivalence factor required in the NRL methodology for the open circuit voltage.

In addition, the analytical model used here provides a simple way to assess the lifetime associated with defect states in the space charge region, only based on dark J-V data. The inherent limitations are the inability to distinguish between electron and hole traps and the insensitivity to defects far from the intrinsic Fermi level. The influence of defect levels further away than 0.35 to 0.4 eV from the intrinsic level will show their effect at voltages around 0.8 V according to Equation 23 and for the cells used in this work are masked by either the diffusion component or series resistance effects.

To perform the same analysis at low temperatures could be a suitable approach to reveal the presence of additional defect levels far away from the midgap position. In addition, such an analysis might be helpful in explaining degradation mechanisms encountered by space solar cells when operating in low-temperature conditions, typical for deep-space missions.

ORCID

Carmine Pellegrino https://orcid.org/0000-0003-2533-1036
Claus G. Zimmermann https://orcid.org/0000-0003-2574-1676

REFERENCES

1. Hoheisel R, Scheiman D, Messenger S, Jenkins P, Walters R. Detailed characterization of the radiation response of multijunction solar cells using electroluminescence measurements. *IEEE Trans Nucl Sci*. 2015;62(6):2894-2898.
2. Meusel M, Baur C, Guter W, Hermle M. "Development status of European multi-junction space solar cells with high radiation hardness," *Proc. 20th EPSEC*, no. August, 2005.
3. Messenger SR, Summers GP, Burke EA, Walters RJ, Xapsos MA. Modeling solar cell degradation in space: a comparison of the NRL displacement damage dose and the JPL equivalent fluence approaches. *Prog Photovoltaics Res Appl*. 2001;9(2):103-121.
4. Zimmermann CG. Utilizing lateral current spreading in multifunction solar cells: An alternative approach to detecting mechanical defects. *J Appl Phys*. 2006;100(2):023714.
5. "ECSS-E-ST-20-08C," *Sp. Eng. - Photovoltaics Assem. components*, no. July, 2012:1–197.
6. Ziegler JF, Ziegler MD, Biersack JP. SRIM - the stopping and range of ions in matter (2010). *Nucl Instruments Methods Phys Res Sect B Beam Interact with Mater Atoms*. 2010;268(11–12):1818-1823.
7. Leroy C, Rancoita P-G. *Principles of Radiation Interaction in Matter and Detection*. Singapore: World Scientific Publishing Co. Pte. Ltd.; 2009.
8. Baur C, Gervasi M, Nieminen P, Rancoita PG, and Tacconi M. "Solar Cell Degradation Analysis Applying the Displacement Damage Dose Approach Using Appropriate Niel Values," *Eur. Sp. Power Conf. 2014*, no. April, 2014.
9. Salzberger M, Nömayr C, Lugli P, Messenger SR, Zimmermann CG. Degradation fitting of irradiated solar cells using variable threshold energy for atomic displacement. *Prog Photovoltaics Res Appl*. 2017;25(9):773-781.
10. Shockley W. The theory of p-n junctions in semiconductors and p-n junction transistors. *Bell Syst Tech J*. 1949;28(3):435-489.
11. Sze SM, Ng KK. *Physics of Semiconductor Devices*. 3rd ed. New York: John Wiley Sons, Inc.; 2007:164-682.
12. Sah C, Noyce RN, Shockley W. Carrier generation and recombination in P-N junctions. *Proc. IRE*. 1956;1:1228-1243.
13. Salzberger M, Rutzinger M, Nömayr C, Lugli P, Zimmermann CG. Voltage-dependent photocurrent in irradiated GaAs solar cells. *Prog Photovoltaics Res Appl*. 2018;1-9.
14. Anspaugh BE. *GaAs Solar Cell Radiation Handbook*," National Aeronautics and Space Administration. Jet Propulsion Laboratory, California Institute of Technology; 1996.
15. Cappelletti MA, Casas GA, Morales DM, Hasperue W, Blancá ELPY. Study of the electrical parameters degradation of GaAs sub-cells for triple junction space solar cells by computer simulation. *Semicond Sci Technol*. 2016;31(11):115020.
16. Wolf M, Noel GT, Stirn RJ. Investigation of the double exponential in the current-voltage characteristics of silicon solar cells. *IEEE Trans Electron Devices*. 1977;ED-24(4):419-428.
17. Imaizumi M, Nakamura T, Takamoto T, Ohshima T, Tajima M. Radiation degradation characteristics of component subcells in inverted metamorphic triple-junction solar cells irradiated with electrons and protons. *Prog Photovoltaics Res Appl*. 2017;25(2):161-174.
18. Shockley W, Read WT. Statistics of the recombination of holes and electrons. *Phys Rev*. 1952;87(46):835-842.
19. Schneider B, Strutt MJ. Theory and experiments on shot noise in silicon P-N junction diodes and transistors. *Proc IRE*. 1959;47(4):546-554.
20. Choo SC. Carrier generation-recombination in the space-charge region of an asymmetrical p-n junction. *SolidState Electron*. 1968;11(11):1069-1077.
21. Choo S. On space-charge recombination in pn junctions. *Solid State Electron*. 1996;39(2):308-310.
22. Corkish R, Green MA. Junction recombination current in abrupt junction diodes under forward bias. *J Appl Phys*. 1996;80(5):3083-3090.
23. Pallarès J, Marsal LF, Correig X, Calderer J, Alcubilla R. Space charge recombination in P-N junctions with a discrete and continuous trap distribution. *Solid State Electron*. 1997;41(1):17-23.
24. Chen XJ, Barnaby HJ, Warner JH, Messenger SR, Walters RJ, Ringel SA, Park J. "Non-linear behaviors of dark current slope in P^+N GaAs solar cells following proton irradiations," *Photovolt Spec Conf (PVSC), 2009 34th* IEEE, 2009:1565–1570.

25. Rao A, Krishnan S, Sajeev G, Siddappa K. Temperature and 8 MeV electron irradiation effects on GaAs solar cells. *Pramana - J Phys*. 2010;74(6):995-1008.

26. Ponst D, Bourgoin JC. Irradiation-induced defects in gaas. *Journal of Physics C: Solid State Physics*. 1985;18(20):3839-3871.

27. Stievenard D, Boddaert X, Bourgoin JC. Irradiation-induced defects in p-type GaAs. *Phys Rev B*. 1986;34(6):4048-4058.

28. Bourgoin JC, Zazouiu M. Irradiation-induced degradation in solar cell: Characterization of recombination. *Semicond Sci Technol*. 2002;17(5): 453-460.

29. Brunkov PN, Kalinovsky VS, Nikitin VG, Sobolev MM. Generation of the EL2 defect in n-GaAs irradiated by high energy protons. *Semicond Sci Technol*. 1992;7(10):1237-1240.

How to cite this article: Pellegrino C, Gagliardi A, Zimmermann CG. Difference in space-charge recombination of proton and electron irradiated GaAs solar cells. *Prog Photovolt Res Appl*. 2019;1–12. https://doi.org/10.1002/pip.3100